

RESEARCH ARTICLE

Nonalcoholic Fatty Liver Disease: Correlation of the Liver Parenchyma Fatty Acid with Intravoxel Incoherent Motion MR Imaging—An Experimental Study in a Rat Model

Seung-Man Yu^{1,2}, Sung Hwan Ki³, Hyeon-Man Baek^{4*}

1 Department of Biomedical Engineering, Research Institute of Biomedical Engineering, College of Medicine, The Catholic University of Korea, Seoul, Korea, **2** Department of Radiological Science, Gimcheon University, Gimcheon, Gyeongsangbuk-do, Korea, **3** Department of Toxicology, College of pharmacy, Chosun University, Gwangju, Korea, **4** Korea Basic Science Institute, Yeongudanji-Ro, Ochang-eup, Cheongwon-gun, Chungbuk, Korea

* hmbaek@kbsi.re.kr



OPEN ACCESS

Citation: Yu S-M, Ki SH, Baek H-M (2015) Nonalcoholic Fatty Liver Disease: Correlation of the Liver Parenchyma Fatty Acid with Intravoxel Incoherent Motion MR Imaging—An Experimental Study in a Rat Model. PLoS ONE 10(10): e0139874. doi:10.1371/journal.pone.0139874

Editor: Zhuoli Zhang, Northwestern University Feinberg School of Medicine, UNITED STATES

Received: April 7, 2015

Accepted: August 31, 2015

Published: October 13, 2015

Copyright: © 2015 Yu et al. This is an open access article distributed under the terms of the [Creative Commons Attribution License](https://creativecommons.org/licenses/by/4.0/), which permits unrestricted use, distribution, and reproduction in any medium, provided the original author and source are credited.

Data Availability Statement: All relevant data are within the paper and its Supporting Information files.

Funding: This paper was supported in part by the Korea Basic Science Institute (KBSI) Grant No. E35436 and E35600 and the Basic Science Research program through the National Research Foundation of Korea (NRF) funded by the Ministry of Science, ICT & Future Planning (2015R1C1A1A02036988).

Competing Interests: The authors have declared that no competing interests exist.

Abstract

Purpose

To prospectively evaluate the changes in fatty acid concentration after administrating a 60% high-fat diet to a non-alcoholic fatty liver disease rat model and to perform a correlation analysis between fatty acid with molecular diffusion (D_{true}), perfusion-related diffusion (D_{fast}), and perfusion fraction (P_{fraction}).

Material and Methods

This prospective study was approved by the appropriate ethics committee. Ten male Sprague-Dawley rats were fed a 60% high-fat diet until the study was finished. Point-resolved spectroscopy sequence ¹H-MRS with TR = 1,500 msec, TE = 35 msec, NEX = 64, and 8×8×8 mm³ voxel was used to acquire magnetic resonance spectroscopy (MRS) data. Diffusion-weighted imaging was performed on a two-dimensional multi-b value spin echo planar image with the following parameters: repetition time msec/echo time msec, 4500/63; field of view, 120×120 msec²; matrix, 128×128; section thickness, 3 mm; number of repetition, 8; and multiple b value, 0, 25, 50, 75, 100, 200, 500, 1000 sec/mm². Baseline magnetic resonance imaging and magnetic resonance spectroscopy data (control) were acquired. ¹H proton MRS and diffusion-weighted imaging were obtained every 2 weeks for 8 weeks. The individual contributions of the true molecular diffusion and the incoherent motions of water molecules in the capillary network to the apparent diffusion changes were estimated using a least-square nonlinear fitting in MatLab. A Wilcoxon signed-rank test with the Kruskal-Wallis test was used to compare each week's fatty acid mean quantification. Spearman's correlation coefficient was used to evaluate the correlation between each fatty acid (e.g., total lipid (TL), total saturated fatty acid (TSFA), total unsaturated fatty acid (TUSFA), total

unsaturated bond (TUSB), and polyunsaturated bond (PUSB)) and intravoxel incoherent motion (IVIM) mapping images (e.g., D_{true} , D_{fast} , and P_{fraction}).

Results

The highest mean TL value was at week 8 (0.278 ± 0.10) after the administration of the 60% high-fat diet, followed by weeks 6, 4, 2, and 0. The concentration level (16.99 ± 2.29) of TSFA at week 4 was the highest. No significant differences in the concentrations of TUSFA, TUSB, or PUSB were observed in different weeks.

Conclusion

After the administration of the 60% high-fat diet in nonalcoholic fatty liver disease model, TL and TSFA depositions had significant changes. The mean concentrations of TUSFA, TUSB, PUSB did not significantly change. Total unsaturated fatty acid and polyunsaturated bond showed positive correlations with D_{true} and P_{fraction} .

Introduction

Non-alcoholic fatty liver is a common disease that is currently experienced by 10–24% of the world's population [1]. It can progress into chronic liver diseases such as liver fibrosis and cirrhosis [2–4]. In the USA, 32–37% of nonalcoholic fatty liver disease (NAFLD) patients progress to liver fibrosis in 3–6 years, with 12% experiencing liver cirrhosis in 8–10 years [5–8]. A simple scoring system for predicting cirrhosis in nonalcoholic fatty liver disease has been used that measured platelet, albumin, and AST/ALT ratios in blood samples [9]. NAFLD is usually associated with metabolic syndromes (MetS), such as type 2 diabetes, insulin resistance, hypertension, and dyslipidemia, that are accompanied by abdominal obesity [10–11]. Accordingly, clinical approaches to investigating the relationship between NAFLD and the prevalence of atherosclerosis and cardiovascular disease have been conducted [12]. NAFLD is not a simple risk factor of type 2 diabetes, cardiovascular disease, or liver cirrhosis.

Liver biopsy has been accepted as the gold standard for diagnosing NAFLD. However, liver biopsy is not only invasive but also clinician-dependent, which often causes sampling errors [13]. Moreover, it is impossible to use this method over a long period to monitor the progress of NAFLD. In a 2014 study, Davide et al. examined whether extracellular vesicles are increased in the liver and blood during experimental NAFLD during searches for bio-markers [14]. Magnetic resonance spectroscopy (MRS) has been widely used to diagnose NAFLD [15–18]. MRS is a noninvasive and *in vivo* method with high sensitivity and specificity. It is frequently used to diagnose various diseases such as NAFLD, liver fibrosis, and cirrhosis [19–22]. Total lipid (TL), total saturated fatty acid (TSFA), total unsaturated fatty acid (TUSFA), total unsaturated bond (TUSB), and polyunsaturated bond (PUSB) can be calculated with liver fatty acid analysis using ^1H -MRS through the signal integration of lipid methyl protons ($-\text{CH}_3$, 0.9 ppm), methylene protons ($(-\text{CH}_2-)_n$, 1.3 ppm), allylic protons ($-\text{CH}_2-\text{C}=\text{C}-\text{CH}_2-$, 2.0 ppm), diallylic protons ($=\text{C}-\text{CH}_2-\text{C}=\text{C}$, 2.8 ppm), and methene protons ($-\text{CH}=\text{CH}-$, 5.3 ppm) [19]. Many studies have been conducted on fatty acid deposition in liver parenchyma and fatty acid changes in liver fibrosis using animal models [19, 23].

Diffusion-weighted imaging (DWI) techniques have been recently attempted for diagnosing fatty liver, liver fibrosis, and cirrhosis [24–26]. In particular, the intravoxel incoherent motion

(IVIM) is a method of obtaining multi b values to encompass both low- b -value and high- b -value diffusion-weighted images to reflect the random microscopic motion that occurs in voxels on MRI of either intracellular or extracellular water molecules and the micro-circulation of blood through non-linear bi-exponential graph fitting [27]. Previous studies have shown that pure molecular diffusion and perfusion fraction values in the liver parenchyma of liver fibrosis or cirrhosis were lower than those in a control group [24–28]. In fatty liver patients, fat deposition in the liver parenchyma was similar to that in liver fibrosis patients because of distortion and sinus compression of the microcirculatory anatomy and reduced pure molecular diffusion [27–28]. However, the correlation of changes in fatty acid in the liver parenchyma with fat deposition and true diffusion with blood microcirculation has not yet been studied.

Therefore, the objectives of this study were to examine the changes in fatty acid concentration after high-fat diet administration and to determine factors that affect NAFLD through correlation analysis between fatty acid and pure molecular diffusion (D_{true}), perfusion-related diffusion (D_{fast}), or perfusion fraction (P_{fraction}).

Materials and Methods

This study was carried out in strict accordance with the recommendations in the Guide for the Care and Use of Laboratory Animals of the National Institutes of Health. The protocol was approved by the Committee on the Ethics of Animal Experiments of the Korea Basic Science Institute (KBSI-AEC 1305). All surgery was performed under sodium pentobarbital anesthesia, and all efforts were made to minimize suffering.

Animal Model

Ten male 8-week-old Sprague-Dawley rats that weighed 100–150 g were housed with ad libitum access to water. The animal care facility was controlled for humidity and temperature on a 12 h light-dark schedule. All Sprague-Dawley rats were fed a 60% high-fat diet that contained 60% fat, 20% protein, and 20% carbohydrate (D12492, Research Diets, New Brunswick, NJ) until the experiment was complete [29]. Baseline MRI and MRS data were acquired before the rats were fed the high-fat diet. MRI and MRS data were also acquired every 2 weeks for 8 weeks according to the schedule of the ^1H -MRS experiments. The experimental rats were anesthetized for all surgical and imaging procedures by general inhalation anesthesia (isoflurane 1.5 to 2.5% vol., plus O_2). After completion of the imaging study, mice were sacrificed under deep anesthesia and the livers were excised and processed for further histological analysis.

In vivo Liver ^1H MRS

All MRI and ^1H -MRS experiments were performed on a 3.0 Tesla MRI scanner (Achiva Tx 3.0 T; Philips Medical Systems, Netherlands) with a maximum gradient of 200 mT/m using a 4-channel animal coil (CG-MUC18-H300-AP, Shanghai Chenguang Medical Technologies Co., Ltd., China). During liver MRS and imaging, all NAFLD model rats were anesthetized with isoflurane/air at 1.0 to 1.5% via a nose cone with respiratory monitoring [30]. Using T_2 -weighted fast spin echo, whole liver parenchyma images were acquired in three transverse axial (FOV 60 mm×60 mm, slice thickness = 1.5 mm), coronal (FOV 6 cm×6 cm, slice thickness = 1.5 mm), and sagittal (FOV 6 cm×6 cm, slice thickness = 1.5 mm) planes to localize voxels or volume of interest for MRS.

We used a point-resolved spectroscopy (PRESS) sequence for localized ^1H -MRS with TR = 1,500 msec, TE = 35 msec, NEX = 64, and total scan time = 10 minute. An $8\times 8\times 8\text{ mm}^3$ voxel was placed within a homogeneous liver parenchyma to avoid large blood vessels, as shown in Fig 1.

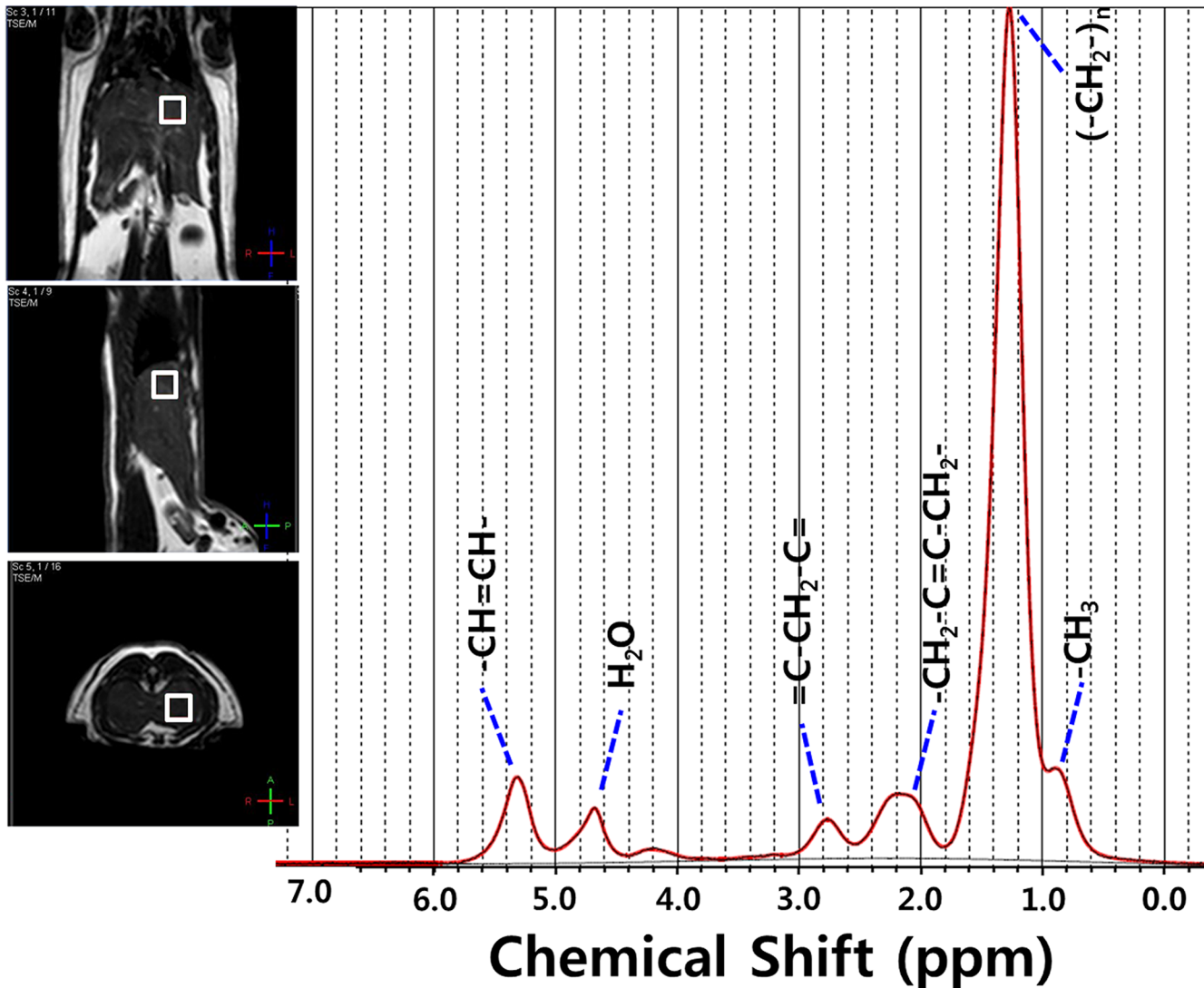


Fig 1. In-vivo MRS analysis. Typical liver ^1H proton magnetic resonance spectroscopy spectra at week 8 after the start of the high-fat diet administration, with typical voxel ($0.8 \times 0.8 \times 0.8 \text{ cm}^3$) placement, were shown in the T_2 -weighed axial, sagittal and coronal turbo spin images. The water (H_2O) and 4.7 ppm signals were effectively suppressed in the spectra.

doi:10.1371/journal.pone.0139874.g001

We applied iterative VOI shim [31]. The water signal of each VOI was suppressed by variable pulse power and optimized relaxation delays before the scan. The signal was shimmed to a line width of lipid (4 to 6 Hz) over VOI (30).

IVIM MR imaging

The multi b value DWI was conducted immediately after the ^1H -MRS data were obtained by using the same MR system. Whole liver parenchyma transverse axial images were obtained. DWI was performed on a two-dimensional multi-b value spin echo planar imaging with the following parameters: prepetition time /echo time, 4500 /63 msec; field of view, $120 \times 120 \text{ mm}^2$; matrix, 128×128 ; section thickness, 3 mm; number of repetition, 8; and multiple b value, 0, 25, 50, 75, 100, 200, 500, and 1000 sec/mm^2 . Individual contributions of true molecular diffusion and incoherent motions of water molecules in the capillary network to the apparent diffusion

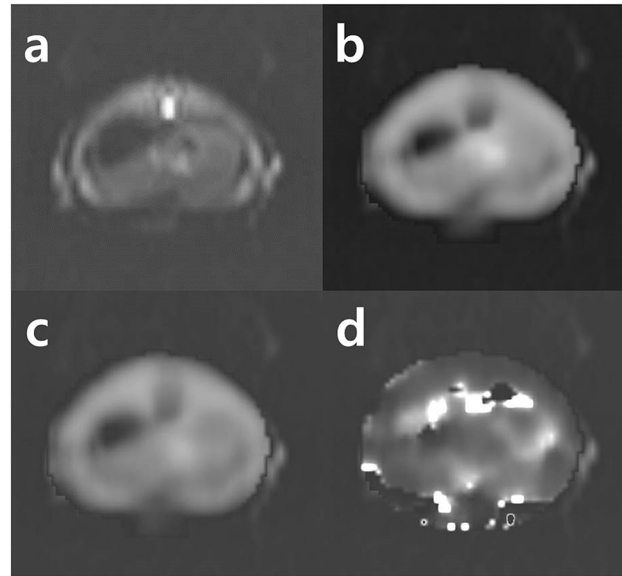


Fig 2. Week 4 NAFLD IVIM data mapping image of rat. (a) Axial diffusion-weighted image of liver ($b = 200 \text{ sec/mm}^2$); (b) D_{fast} mapping image; (c) D_{true} mapping image; (d) P_{fraction} mapping image.

doi:10.1371/journal.pone.0139874.g002

changes, D_{true} , D_{fast} , and P_{fraction} were estimated as shown in Fig 2 using a least-square nonlinear fitting in MatLab (Mathworks, Natick, MA, USA) by fitting, pixel by pixel, the DWI signal decay in the region of interest (ROI) to the IVIM by-compartmental model as follows: $SI/SI_0 = (1 - P_{\text{fraction}}) \times \exp(-bD_{\text{true}}) + P_{\text{fraction}} \times \exp(-bD_{\text{fast}})$, where SI was the signal intensity and P_{fraction} was the perfusion fraction linked to blood volume.

Histology

After 8 weeks of MRI and ^1H -MRS study, all rats were sacrificed for histological evaluation. One additional normal animal was sacrificed as a control. All liver specimens were fixed in formalin, embedded in paraffin, sectioned, and examined under light microscopy after standard hematoxylin-eosin staining and Prussian blue staining to confirm fat and iron deposition in the liver parenchyma.

MRS Analysis

Raw ^1H -MRS data were analyzed using LCModel software (version 6.3-1H, Stephen W. Provencher). Spectrum type with lipid-11 was selected for quantifying all lipids, with water data as references. All lipid peaks were automatically calculated in LCModel. The LC model parameters were set according to the LCModel & LCMgui user's manual (<http://s-provencher.com/pages/lcm-manual.shtml>). Less than 10% standard deviation (%SD) of metabolite quantification data was allowed. The %SD called the Cramér-Rao lower bound of useful reliability indicators was used for error estimates. The integrating areas under peaks were measured as follows: signal integrals in lipid methyl protons at 0.90 ppm, methylene proton at 1.30 ppm, allylic protons at 2.02 ppm, diallylic protons at 2.77 ppm, and methane protons at 5.30 ppm. For relative quantification, total lipid ($(-\text{CH}_2-)_n$ / noise), total saturated fatty acid, total unsaturated fatty acid, total unsaturated bond, and polyunsaturated bond were quantified by separating each peak area of $(-\text{CH}_2-)_n$, $-\text{CH}_2-\text{C}=\text{C}-\text{CH}_2-$, $=\text{C}-\text{CH}_2-\text{C}=\text{C}-$, and $-\text{CH}=\text{CH}-$ by $-\text{CH}_3$ as shown in Table 1.

Table 1. Peak Area Ratios of Various Metabolite Indices Measured by Proton Magnetic Resonance Spectroscopy (¹H-MRS).

Index	Peak Area Ratio	Frequency
Total lipid	(-CH ₂ -)/n/water	1.3/4.7 ppm
Total saturated fatty acid	3(-CH ₂ -)/2(-CH ₃)	1.3/0.9 ppm
Total unsaturated fatty acid	3(-CH ₂ -C = C-CH ₂ -)/4(-CH ₃)	2.0/0.9 ppm
Total unsaturated bond	3(-CH = CH-)/2(-CH ₃)	5.3/0.9 ppm
Polyunsaturated bond	3 (= C-CH ₂ -C =) /2(-CH ₃)	2.8/0.9 ppm

doi:10.1371/journal.pone.0139874.t001

IVIM MR Analysis

Extracted mapping imaging diffusion coefficient, pseudo diffusion coefficient, and perfusion fraction were analyzed using standard software on the workstation. All ROIs were manually positioned by one author (Yu). The region of interest of each image was a set circle in the right lobe that was just about the same as the VOI region of MRS. Every ROI size was manipulated differently during measurement to avoid IVIM mapping imaging artifacts. The Wilcoxon signed-rank test with the Kruskal-Wallis test was used to compare each week's fatty acid mean quantifications with significance level $p < 0.05$. Results are expressed as mean \pm standard deviation. Spearman's correlation coefficient was used to evaluate the correlations between each fatty acid (e.g., TL, TSFA, TUSFA, TUSB, and PUBS) and IVIM mapping images (e.g., D_{true} , D_{fast} , and $P_{fraction}$) with a significance level of $p < 0.05$. All statistical analyses were performed using SPSS version 20.0 (SPSS Incorporated, Chicago, IL, USA).

Results

Comparison of the mean of hepatic fatty acids

The differences in the N number shown under the X axis (Fig 3) were observed because 10% or lower % SD values were used.

The highest mean TL value was measured at week 8 (0.278 ± 0.10) after the administration of the 60% high-fat diet, followed by weeks 6, 4, 2, and 0. The TL value at week 2 was 0.201 ± 0.07 , which was insignificantly ($p > 0.05$) lower than that of week 8. The TL value increase at week 2 from baseline week 0 was the most significant ($p < 0.01$) among all of the increases. The mean increases in the TL value at weeks 2 and 4 were also significant ($p < 0.05$). The TSFA concentration level (16.99 ± 2.29) at week 4 was the highest. A statistically significant mean difference in the levels was observed only between the baseline and week 2 ($p < 0.05$). No significant differences in the concentration levels of TUSFA, TUSB, or polyunsaturated bond PUBS were observed among different weeks.

Correlation between hepatic fatty acid and IVIM mapping images

The results of the non-parametric analysis of the correlations between hepatic fatty acid and IVIM mapping images are summarized in Table 2.

A correlation between total lipid and D_{fast} was observed ($r = 0.333$, $p < 0.05$). $P_{fraction}$ had no correlation with TL. TUSFA showed a positive correlation with D_{true} . PUBS was significantly correlated with D_{fast} ($r = 0.413$, $p < 0.01$) and $P_{fraction}$ ($r = 0.346$, $p < 0.05$) in the liver parenchyma, confirming that D_{fast} and $P_{fraction}$ are closely related to liver parenchymal microcirculation. PUBS also correlated with D_{true} ($r = 0.413$, $p < 0.05$, Fig 4).

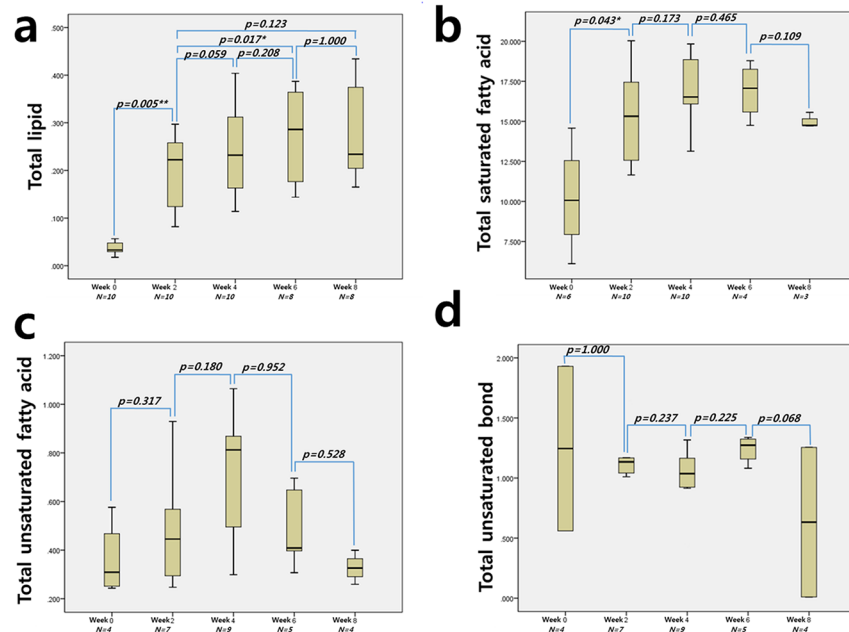


Fig 3. The mean differences from the fatty acid comparisons of each week's mean quantification. The total lipid and TSFA showed the highest concentrations at weeks 8 and 6, respectively. There were no significant mean differences in TUSFA, TUSB, or PUSB in any of the weeks.

doi:10.1371/journal.pone.0139874.g003

Histologic features

As shown in Fig 5, complete fat deposition in the liver parenchyma was observed in the liver biopsy of a Sprague-Dawley rat through hematoxylin and eosin stain. In the Prussian blue staining observation, iron deposition was not confirmed in any liver tissue.

Discussion

In this study, changes in fatty acid with fat deposition were observed in liver parenchyma. Correlations among fatty acid, intracellular or extracellular water molecules, and blood microcirculation were investigated. As the NAFLD progresses into chronic liver diseases such as liver fibrosis and cirrhosis, the fat deposition in the liver parenchyma is known to have a negative effect on micro-circulation. In this study, there was great significance in revealing the specific fatty acid through the correlate fatty acid and representing the micro-circulation factor (D_{true} , D_{fast} and $P_{fraction}$) in NAFLD.

Table 2. Spearman correlation analysis between hepatic fatty acid and IVIM data mapping images.

	D_{fast}	D_{true}	$P_{fraction}$
Total lipid (n = 46)	0.333 ($p = 0.012^*$)	0.238 ($p = 0.055$)	0.059 ($p = 0.349$)
otal saturated fatty acid (n = 30)	0.210 ($p = 0.124$)	0.260 ($p = 0.082$)	0.194 ($p = 0.152$)
Total unsaturated fatty acid (n = 28)	0.129 ($p = 0.252$)	0.535 ($p = 0.002^{**}$)	0.359 ($p = 0.030^*$)
Total unsaturated bond (n = 22)	0.159 ($p = 0.240$)	-0.014 ($p = 0.475$)	0.089 ($p = 0.347$)
Poly unsaturated bond (n = 31)	0.413 ($p = 0.010^{**}$)	0.413 ($p = 0.011^*$)	0.346 ($p = 0.028^*$)

** $p < 0.01$

* $p < 0.05$

doi:10.1371/journal.pone.0139874.t002

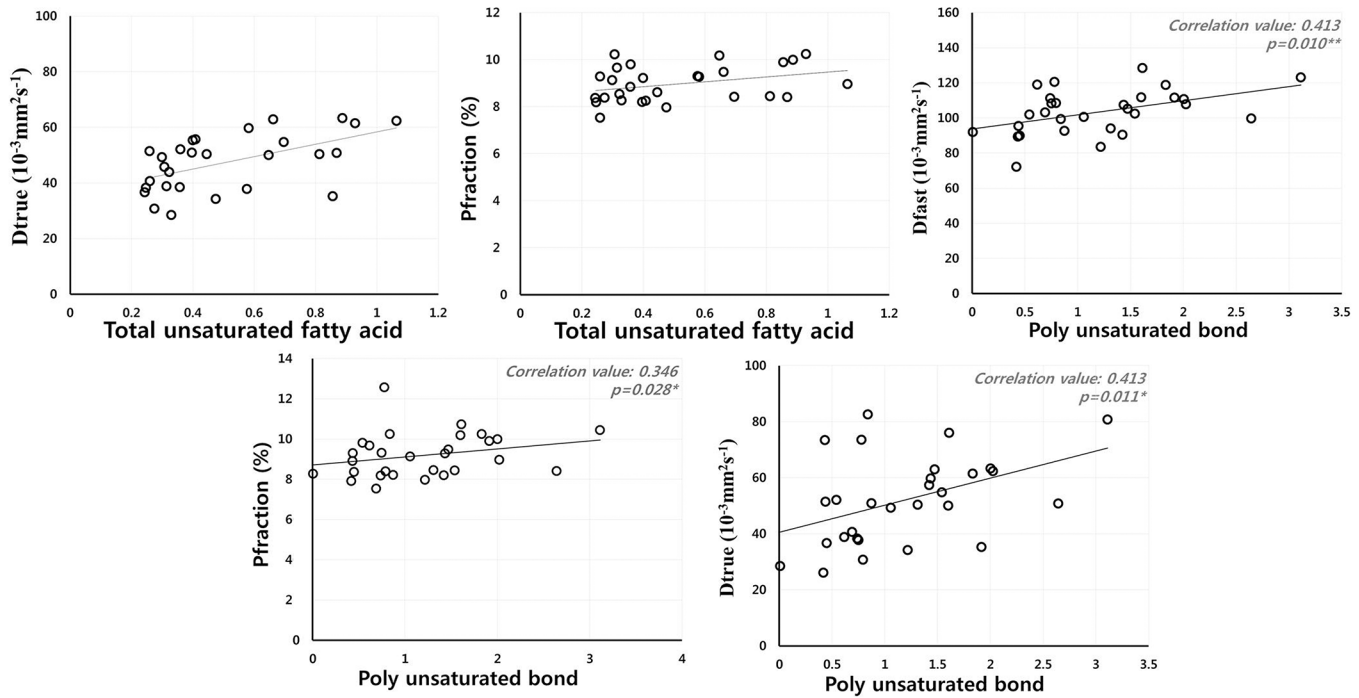


Fig 4. Correlation coefficient values between IVIM mapping data and TUSFA and PUBS. The TUSFA and PUBS had significant correlations with D_{true} and $P_{fraction}$. Blood perfusion TUSB and PUBS in the intravascular compartment with volume fraction ($P_{fraction}$) is described by the pseudorandom blood perfusion (D_{fast}), in which the extra vascular compartment is described by the true molecular diffusion (D_{true}).

doi:10.1371/journal.pone.0139874.g004

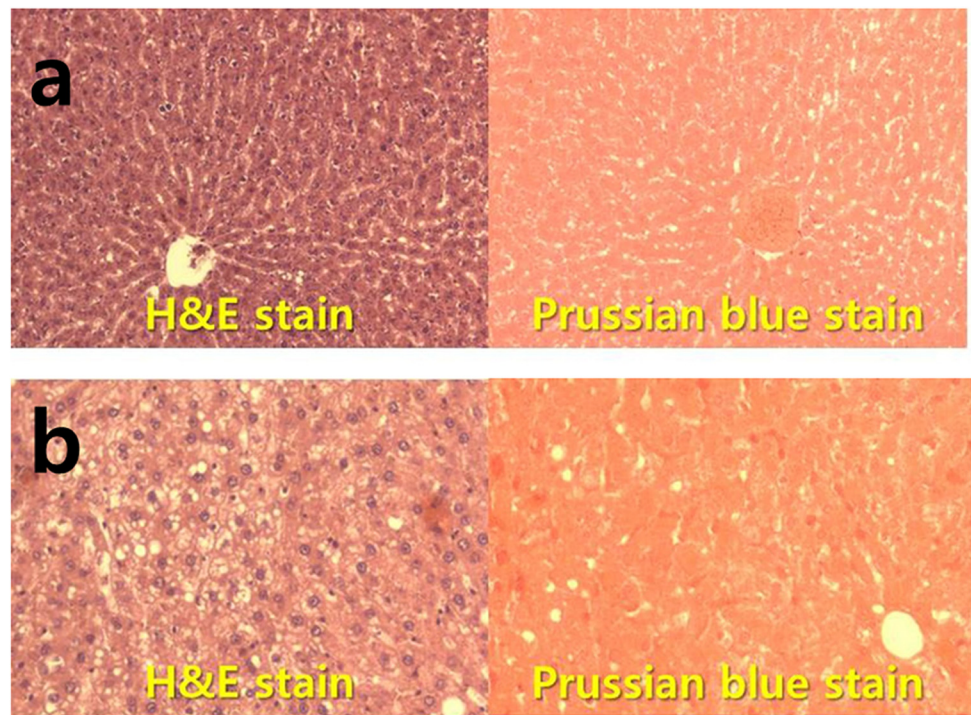


Fig 5. Hematoxylin/eosin and Prussian blue stained histology sections of liver form. (a) Rat not fed with the 60% high-fat diet ($\times 100$), (b) nonalcoholic fatty liver rat model fed with the high-fat diet after 8 weeks.

doi:10.1371/journal.pone.0139874.g005

After the administration of a 60% high-fat diet, the TL level consistently increased, with the peak at week 8. However, the mean difference between week 6 and week 8 was statistically insignificant. TL concentration was saturated at week 6. The NAFLD modeling through the high-fat diet was completed at week 6 and afterwards.

The TSFA concentration calculated through the 1.3 ppm and 0.9 ppm lipid proton ratio increased consistently from week 0 to week 4 and decreased thereafter. The mean difference in TSFA concentrations between week 2 and afterwards was statistically insignificant. The mean levels of TUSFA and PUSB increased from week 0 to week 6 and decreased thereafter. However, the differences were statistically insignificant. The mean differences in TUSB concentrations were also statistically insignificant. Changes in TL and TSFA deposition were the most significant after the administration of the 60% high-fat diet, whereas the changes in the other unsaturated acids and bonds were insignificant. Excellent liver fat deposition was confirmed after hematoxylin-eosin staining for histological evaluation. According to studies by Pacifico et al. [32] and Scorletti et al. [33], the administration of n-3 PUFA positively affected Mets and NAFLD [32–33]. In this study, the long-term administration of the 60% high-fat diet did not affect the changes in PUFA, TUSFA, or TUSB. Therefore, a high-fat diet might be an indirect factor that could adversely affect the liver.

Studies on liver diseases using DWI have been conducted previously [25–28, 34]. Particularly, D_{true} , D_{fast} , and P_{fraction} data can be analyzed by applying various b-values on the same slice using signal reduction in the low and high b-values through bi-exponential data fitting. In previous studies, a slightly negative correlation between the increase in fat fraction value and the D_{true} value was confirmed with statistical significance [29]. In another study, D_{true} and D_{fast} values were low in the hepatic steatosis group without hepatic steatosis [28]. Based on the results of previous studies, the TL and TSFA were expected to show negative correlations with D_{true} and D_{fast} because the liver fat content calculation from the equation of Guiu et al. $(100 \cdot \text{CH}_2)/(\text{CH}_2 + \text{water})$ was similar to the TL in this study, which was calculated using the 1.3 ppm proton lipid metabolite and water ratios. In this study, no fatty acid showed a correlation with D_{true} . Rather, a low correlation was observed between total lipid and D_{fast} ($r = 0.333$, $p < 0.05$). The etiology in the previous studies that targeted human bodies differed from that in other studies because of fat deposition caused by type *b* and *c* type hepatitis as well as by the fatty liver that was induced by the administration of the high-fat diet. Accordingly, studies on microcirculation in the liver parenchyma according to the type of fatty acid caused by etiology are required. In a 2014 study by Joo et al. that used a NAFLD rabbit model, the D_{true} value in the severe NAFLD group decreased slightly without statistical significance. However, D_{fast} decreased significantly [35]. Because the NAFLD model P_{fraction} reflects the capillary perfusion contribution in ADC, the D_{true} reduction and the D_{fast} increase might have been influenced by the fattening equation that meant a P_{fraction} decrease. The positive correlation of D_{true} with D_{fast} in this study could have been for the same reason. The high D_{true} meant an increase in the pure water diffusivity and in the capillary perfusion [28, 35]. In this study, the fatty acid that showed a positive correlation with D_{true} and P_{fraction} was TUSFA. The correlation coefficient with D_{true} was 0.535 ($p < 0.01$), a significantly high correlation. A positive correlation with P_{fraction} was also confirmed with statistical significance. The increase in the pure water diffusivity positively affected capillary perfusion. In particular, PUSB was confirmed to have positive correlations with D_{fast} , D_{true} , and P_{fraction} with statistical significance. The positive correlation between D_{fast} and P_{fraction} was attributed to the fact that D_{fast} represented the perfusion-related incoherent micro-circulation whereas P_{fraction} represented the blood volume. In a study by Monteiro J et al. [36], n-6 and n-3 polyunsaturated fatty acids had beneficial effects on cardiovascular diseases and non-alcoholic fatty liver diseases. In this study, positive effects on D_{fast} , D_{true} , and P_{fraction} in USFA and PUSB were confirmed. However, the mean concentrations of USFA and

PUSB did not significantly increase after the administration of the 60% high-fat diet. Additional studies on the positive effects of increased TUSFA and PUSB concentrations on blood perfusion in liver parenchyma are merited.

The limitations of this study are as follows: For accurate metabolite quantifications, spin-lattice (T_1) and spin-spin (T_2) relaxation must be corrected. T_2^* correction and accurate fat fraction calculation using chemical shift imaging techniques have been attempted not only in MRS but also in multi-echo Dixon [37–41]. In a study by Andrew et al., new methods of *in vivo* T_2 time measurement through echo-time averaging were suggested [42]. Iron deposition in the liver parenchyma was confirmed to be one of the major factors that triggered T_2^* that was closely correlated with the development of liver fibrosis and cirrhosis [43–45]. In the fatty liver model in this study, iron deposition through Prussian blue staining did not occur at week 8 or afterwards. The absence of T_2^* correction for accurate metabolite quantification was the most significant limitation of this study.

Conclusions

In conclusion, the administration of the 60% high-fat diet to rats gradually increased the TL and TSFA levels in the liver parenchyma, after which the liver parenchyma became saturated. In the meantime, the levels of TUSFA, TUSFB, and PUSB did not show statistically significant changes. The fatty acids that showed positive correlations with D_{true} and P_{fraction} in the liver parenchyma were TUSFA and PUSB.

Supporting Information

S1 Dataset. The raw data of lipid proton concentration MRS and IVIM parameters. The lipid signals were analyzed using the LCModel algorithm, and a fitting error (the standard deviation) was estimated using the Cramer-Rao lower bounds (CRLB) of the signal amplitude (e.g., at 0.9, 1.3, 2.02, 2.77, and 5.30 ppm). In this work, a CRLB threshold of $\leq 10\%$ was used for quality control.

(XLSX)

Author Contributions

Conceived and designed the experiments: SMY SHK HMB. Performed the experiments: SMY HMB. Analyzed the data: SMY SHK HMB. Contributed reagents/materials/analysis tools: SMY HMB. Wrote the paper: SMY SHK HMB.

References

1. Bataller R, Rombouts K, Altamirano J, Marra F. Fibrosis in alcoholic and nonalcoholic steatohepatitis. *Best Pract Res Clin Gastroenterol* 2011; 25: 231–244. doi: [10.1016/j.bpg.2011.02.010](https://doi.org/10.1016/j.bpg.2011.02.010) PMID: [21497741](https://pubmed.ncbi.nlm.nih.gov/21497741/)
2. Anthony SW, Jude O. Nonalcoholic fatty liver disease and lipids. *Curr Opin Lipidol* 2012; 23: 345–352. doi: [10.1097/MOL.0b013e3283541cfc](https://doi.org/10.1097/MOL.0b013e3283541cfc) PMID: [22617751](https://pubmed.ncbi.nlm.nih.gov/22617751/)
3. Stephen AH, Sigurd T, Paul HH. The Natural History of Nonalcoholic Fatty Liver Disease: A Clinical Histopathological Study. *Am J Gastroenterol* 2003; 98: 2042–2047. PMID: [14499785](https://pubmed.ncbi.nlm.nih.gov/14499785/)
4. Ivana M, Vesna L, Sanjin R, Sandra M, Branka SM, Lidija O. Nonalcoholic fatty liver disease (NAFLD)—a new factor that interplays between inflammation, malnutrition, and atherosclerosis in elderly hemodialysis patients. *Clinical Interventions in Aging* 2014; 9: 1295–1303 doi: [10.2147/CIA.S65382](https://doi.org/10.2147/CIA.S65382) PMID: [25143715](https://pubmed.ncbi.nlm.nih.gov/25143715/)
5. Brent ANT, Stephen HC. Nonalcoholic Steatohepatitis: Summary of an AASLD Single Topic Conference. *Hepatology* 2003; 37: 1202–1219. PMID: [12717402](https://pubmed.ncbi.nlm.nih.gov/12717402/)
6. Fassio E, Alvarez E, Domínguez N, Landeira G, Longo C. Natural history of nonalcoholic steatohepatitis: a longitudinal study of repeat liver biopsies. *Hepatology* 2004; 40: 820–826. PMID: [15382171](https://pubmed.ncbi.nlm.nih.gov/15382171/)

7. Adams LA, Sanderson S, Lindor KD, Angulo P. The histological course of nonalcoholic fatty liver disease: a longitudinal study of 103 patients with sequential liver biopsies. *J Hepatol* 2005; 42: 132–138. PMID: [15629518](#)
8. Day CP. Natural history of NAFLD: remarkably benign in the absence of cirrhosis. *Gastroenterology* 2005; 129: 375–378. PMID: [16012969](#)
9. Takaomi K, Yuji O, Masato Y, Kento I, Yoshio E, Hideki F, et al. Simple scoring system for predicting cirrhosis in nonalcoholic fatty liver disease. *World J Gastroenterol* 2014; 20: 10108–10114. doi: [10.3748/wjg.v20.i29.10108](#) PMID: [25110437](#)
10. Ekstedt M, Franzén LE, Mathiesen UL, Thorelius L, Holmqvist M, Bodemar G, et al. Long-term follow-up of patients with NAFLD and elevated liver enzymes. *Hepatology* 2006; 44: 865–873. PMID: [17006923](#)
11. Rafiq N, Bai C, Fang Y, Srishord M, McCullough A, Gramlich T, et al. Long-term follow-up of patients with nonalcoholic fatty liver. *Clin Gastroenterol Hepatol* 2009; 7: 234–238. doi: [10.1016/j.cgh.2008.11.005](#) PMID: [19049831](#)
12. Giovanni T, Guido A. Non-alcoholic fatty liver disease and increased risk of cardiovascular disease. *Atherosclerosis* 2007; 191: 235–240. PMID: [16970951](#)
13. Brunt EM, Kleiner DE, Wilson LA, Unalp A, Behling CE, Lavine JE, et al. Portal chronic inflammation in nonalcoholic fatty liver disease (NAFLD): a histologic marker of advanced NAFLD—Clinicopathologic correlations from the Nonalcoholic Steatohepatitis. *Clinical Research Network. Hepatology* 2009; 49: 809–820. doi: [10.1002/hep.22724](#) PMID: [19142989](#)
14. Povero D, Eguchi A, Li H, Johnson CD, Papouchado BG, Wree A, et al. circulating extracellular vesicles with specific proteome and liver microRNAs are potential biomarkers for liver injury in experimental fatty liver disease. *PLoS One* 9(12): e113651. doi: [10.1371/journal.pone.0113651](#) PMID: [25470250](#)
15. Ren J, Dimitrov I, Sherry D, Malloy CR. Composition of adipose tissue and marrow fat in humans by ¹H NMR at 7 Tesla. *J Lipid Res* 2008; 49: 2055–2062. doi: [10.1194/jlr.D800010-JLR200](#) PMID: [18509197](#)
16. Cassidy FH, Yokoo T, Aganovic L, Hanna RF, Bydder M, Middleton MS, et al. Fatty liver disease: MR imaging techniques for the detection and quantification of liver steatosis. *Radiographics* 2009; 29: 231–260.
17. Hwang JH, Bluml S, Leaf A, Ross BD. In vivo characterization of fatty acids in human adipose tissue using natural abundance ¹H decoupled ¹³C MRS at 1.5 T: clinical applications to dietary therapy. *NMR Biomed* 2003; 16: 160–167. PMID: [12884360](#)
18. Strobel K, Hoff J, Pietzsch J. Localized proton magnetic resonance spectroscopy of lipids in adipose tissue at high spatial resolution in mice in vivo. *J Lipid Res* 2008; 49: 473–480. PMID: [18024705](#)
19. Cheung JS, Fan SJ, Gao DS, BEng, Chow AM, Yang J, et al. In vivo lipid profiling using proton magnetic resonance spectroscopy in an experimental liver fibrosis model. *Acad Radiol* 2011; 18: 377–383. doi: [10.1016/j.acra.2010.10.012](#) PMID: [21167757](#)
20. Zancanaro C, Nano R, Marchioro C, Sbarbati A, Boicelli A, Osculati F. Magnetic resonance spectroscopy investigations of brown adipose tissue and isolated brown adipocytes. *J Lipid Res* 1994; 35: 2191–2199. PMID: [7897317](#)
21. Venkatesh BA, Lima JAC, Bluemke DA, Lai SL, Steenbergen C, Liu CY. MR proton spectroscopy for myocardial lipid deposition quantification: A quantitative comparison between 1.5T and 3T. *J Magn Reson. Imaging* 2012; 36: 1222–1230. doi: [10.1002/jmri.23761](#) PMID: [22826193](#)
22. Runge JH, Bakker PJ, Gaemers IC, Verheil, Hakvoort TBM, Ottenhoff R, et al. Quantitative determination of liver triglyceride levels with 3T ¹H-MR spectroscopy in mice with moderately elevated liver fat content. *Acad Radiol* 2014; 21: 1446–1454. doi: [10.1016/j.acra.2014.06.009](#) PMID: [25300722](#)
23. Corbin IR, Furth EE, Pickup S, Siegelman ES, Delikatny EJ. In vivo assessment of hepatic triglycerides in murine non-alcoholic fatty liver disease using magnetic resonance spectroscopy. *Biochim Biophys Acta* 2009; 1791: 757–763. doi: [10.1016/j.bbaliip.2009.02.014](#) PMID: [19269347](#)
24. Bonekamp S, Torbenson MS, Kamel IR. Diffusion-weighted magnetic resonance imaging for the staging of liver fibrosis. *J Clin Gastroenterol* 2011; 45: 885–892. doi: [10.1097/MCG.0b013e318223bd2c](#) PMID: [21716125](#)
25. Zhou IY, Gao DS, Chow AM, Fan S, Cheung MM, Ling C, et al. Effect of diffusion time on liver DWI: An experimental study of normal and fibrotic livers. *Magn Reson Med* 2014; 72: 1389–1396. doi: [10.1002/mrm.25035](#) PMID: [24258877](#)
26. Hope TA, Ohliger MA, Qayyum A. MR imaging of diffuse liver disease: From technique to diagnosis. *Radiol Clin N Am* 2014; 52: 709–724. doi: [10.1016/j.rcl.2014.02.016](#) PMID: [24889168](#)
27. Gulu B, Petit JM, Capitan V, Aho S, Masson D, Lefevre PH, et al. Intravoxel incoherent motion diffusion-weighted imaging in nonalcoholic fatty liver disease: A 3.0-T MR study. *Radiology* 2012; 265: 96–103. PMID: [22843768](#)

28. Yu SM, Kim SS, Paek MY, Goo EH, Ji YS, Choe BY. Correlation between hepatic fat content using 3-echo 3-D Dixon method and intravoxel incoherent motion (IVIM) perfusion MR imaging. *Appl Magn Reson* 2013; 44: 791–801.
29. Takahashi Y, Soejima Y, Fukusato T. Animal models of nonalcoholic fatty liver disease/ nonalcoholic steatohepatitis. *World J Gastroenterol* 2012; 18: 2300–2308. doi: [10.3748/wjg.v18.i19.2300](https://doi.org/10.3748/wjg.v18.i19.2300) PMID: [22654421](https://pubmed.ncbi.nlm.nih.gov/22654421/)
30. Cheung JS, Guo H, Leung JCK, Man K, Lai KN, Wu EX. MRI visualization of rodent liver structure and peritoneal adhesion with dialyzate enhancement. *Magn Reson Med* 2008; 59: 1170–1174. doi: [10.1002/mrm.21506](https://doi.org/10.1002/mrm.21506) PMID: [18429030](https://pubmed.ncbi.nlm.nih.gov/18429030/)
31. Tkáč I, Starčuk Z, Choi IY, Gruetter R. In vivo ¹H NMR Spectroscopy of rat brain at 1 ms echo time. *Magn Reson Med* 1999; 41: 649–656. PMID: [10332839](https://pubmed.ncbi.nlm.nih.gov/10332839/)
32. Pacifico L, Giansanti S, Gallozzi A, Chiesa C. Long chain omega-3 polyunsaturated fatty acids in pediatric metabolic syndrome. *Mini-Rev Med Chem* 2014; 14: 791–804. PMID: [25307311](https://pubmed.ncbi.nlm.nih.gov/25307311/)
33. Scorletti E, Bhatia L, McCormick KG, Clough GF, Nash K, Calder PC, et al. Design and rationale of the WELCOME trial: A randomized placebo controlled study to test the efficacy of purified long chain omega-3 fatty treatment in non-alcoholic fatty liver disease. *Contemp clin trials* 2014; 37: 301–311. doi: [10.1016/j.cct.2014.02.002](https://doi.org/10.1016/j.cct.2014.02.002) PMID: [24556343](https://pubmed.ncbi.nlm.nih.gov/24556343/)
34. Anderson SW, Soto JA, Milch HN, Ozonoff A, O'Brien M, Hamilton JA, et al. Effect of disease progression on liver apparent diffusion coefficient values in a murine model of NASH at 11.7 tesla MRI 2011; 33: 882–888. doi: [10.1002/jmri.22481](https://doi.org/10.1002/jmri.22481) PMID: [21448953](https://pubmed.ncbi.nlm.nih.gov/21448953/)
35. Joo IJ, Lee JM, Yoon JH, Jang JJ, Han HK, Choi BI. Nonalcoholic fatty liver disease: Intravoxel incoherent motion diffusion-weighted MR imaging—An experimental study in a rabbit model. *Radiology* 2014; 270: 131–140. doi: [10.1148/radiol.13122506](https://doi.org/10.1148/radiol.13122506) PMID: [24091358](https://pubmed.ncbi.nlm.nih.gov/24091358/)
36. Monterio J, Lesle M, Moghadasian MH, Arendt BM, Allard JP, Ma DW. The role of n—6 and n—3 polyunsaturated fatty acids in the manifestation of the metabolic syndrome in cardiovascular disease and non-alcoholic fatty liver disease. *Food Funct* 2014; 5: 426–435. doi: [10.1039/c3fo60551e](https://doi.org/10.1039/c3fo60551e) PMID: [24496399](https://pubmed.ncbi.nlm.nih.gov/24496399/)
37. Kühn JP, Hernado D, Mensel B, Krüger PC, Ittermann T, Mayerle J, et al. Quantitative chemical shift-encoded MRI is an accurate method to quantify hepatic steatosis. *J Magn Reson Imaging* 2014; 39: 1494–1501. doi: [10.1002/jmri.24289](https://doi.org/10.1002/jmri.24289) PMID: [24123655](https://pubmed.ncbi.nlm.nih.gov/24123655/)
38. Yokoo T, Shiehorteza M, Hamilton G, Wolfson T, Schroeder ME, Middleton MS, et al. Estimation of hepatic proton-density fat fraction by using MR imaging at 3.0T. *Radiology* 2011; 258: 749–759. doi: [10.1148/radiol.10100659](https://doi.org/10.1148/radiol.10100659) PMID: [21212366](https://pubmed.ncbi.nlm.nih.gov/21212366/)
39. Lee SJ, Yu SM. Effectiveness evaluation of the fat percentage determination in multi-echo T2-corrected single-voxel spectroscopy by comparing the 3-point Dixon and the 6-point interference Dixon technique. *Appl Magn Reson* 2014; 45: 1333–1342.
40. Meisamy S, Hines CDG, Hamilton G, Sirlin CB, McKenzie CA, Yu H, et al. Quantification of hepatic steatosis with T1-independent, T2*-corrected MR imaging with spectral modeling of fat: Blinded comparison with MR spectroscopy. *Radiology* 2011; 258: 767–775. doi: [10.1148/radiol.10100708](https://doi.org/10.1148/radiol.10100708) PMID: [21248233](https://pubmed.ncbi.nlm.nih.gov/21248233/)
41. Lee SS, Lee YJ, Kim NK, Kim SW, Byun JH, Park SH, et al. Hepatic fat quantification using chemical shift MR imaging and MR spectroscopy in the presence of hepatic iron deposition: Validation in phantoms and in patients with chronic liver disease *J Magn Reson Imaging* 2011; 33: 1390–1398. doi: [10.1002/jmri.22583](https://doi.org/10.1002/jmri.22583) PMID: [21591008](https://pubmed.ncbi.nlm.nih.gov/21591008/)
42. Prescott AP, Shi X, Choi CH, Renshaw P. In vivo T₂ relaxation time measurement with echo-time averaging. *NMR Biomed* 2014; 27: 863–869. doi: [10.1002/nbm.3115](https://doi.org/10.1002/nbm.3115) PMID: [24865447](https://pubmed.ncbi.nlm.nih.gov/24865447/)
43. Sanyal AJ. AGA technical review on nonalcoholic fatty liver disease. *Gastroenterology* 2002; 123: 1705–1725. PMID: [12404245](https://pubmed.ncbi.nlm.nih.gov/12404245/)
44. Bülow R, Mensel B, Meffert P, Hernado D, Evert M, Kühn JP. Diffusion-weighted magnetic resonance imaging for staging liver fibrosis is less reliable in the presence of fat and iron. *Eur Radiol* 2013; 23: 1281–1287. doi: [10.1007/s00330-012-2700-2](https://doi.org/10.1007/s00330-012-2700-2) PMID: [23138385](https://pubmed.ncbi.nlm.nih.gov/23138385/)
45. Shpyleva S, Pogrbna M, Cozart C, Bryant MS, Muskhelishvili L, Tryndyak VP, et al. *J Nutri Biochem* 2014; 25: 1235–1242.